

Damanhour Journal of Pure and Applied Sciences 2025, (1), 7-19



Research Article

Influence of Cu and W Incorporation on the Surface Morphology of MgFe-Layered Double Hydroxides

Gihan M. El-Naggara, Aya M. Kosbaat, Hussein A. Khalafa, E.M.El-Maghrabyb

^aChemistry department, Faculty of Science, Damanhour University, Egypt. ^bPhysics department, Faculty of Science, Damanhour University, Egypt.

*Correspondence: Aya M. Kosba, <u>a.kosba01245@sci.dmu.edu.eg</u> Received: 11 Oct. 2025, Revised: 25 Oct. 2025, Accepted: 29 Oct. 2025, Published: 7 Nov. 2025

Abstract

This research examines the impact of Cu and W incorporation on the surface properties of Mg/Fe-layered double hydroxides (LDHs), with an emphasis on structural, morphological, and thermal changes. Mg/Fe LDH with molar ratio 2/1 and their transition metal-based modification (Cu and W) with molar ratio (1/1/1) for both are prepared. The materials obtained were characterized by TGA, XRD, SEM and BET techniques to reveal structural information regarding both the parent and modified LDH materials. The results revealed multiple stages mass loss, corresponding to dehydration, dehydroxylation, and carbonate decomposition, with the W/Mg/Fe-LDH exhibiting the highest thermal stability and largest residual mass, while Cu/Mg/Fe-LDH showed accelerated decomposition. XRD patterns confirmed the formation of well-crystallized hydrotalcite-like structures with rhombohedral symmetry (R-3m). Metal substitution markedly increased crystallite size from 9.9 nm (Mg/Fe-LDH) to 62.7 nm (Cu/Mg/Fe-LDH) and 70.6 nm (W/Mg/Fe-LDH), indicating enhanced structural ordering. SEM images showed that pristine Mg/Fe-LDH consisted of irregular, loosely packed platelets, whereas Cu and W incorporation produced more compact and uniform morphologies-Cu leading to flake-like aggregates and W yielding dense, spherical nanostructures. N2 adsorptiondesorption analyses indicated type IV isotherms with mesoporous characteristics. The pristine Mg/Fe-LDH exhibited the highest surface area (87 m²/g) and pore volume (0.086 cm³/g), while Cu substitution drastically reduced these values (14 m²/g and 0.015 cm³/g), suggesting pore blocking and densification. The W/Mg/Fe-LDH maintained moderate porosity (38 m²/g, 0.050 cm³/g) with improved pore uniformity. Overall, intercalation of metal significantly influenced the structural, morphological, and textural features of Mg/Fe-LDHs - Cu decreased porosity and thermal stability, whereas W enhanced crystallinity, stability, and mesoporous structure-highlighting their potential for catalysis and adsorption applications.

Keywords: LDH; Textural properties; Porosity; Morphology.

El-Naggar et al 2 of 13

1. Introduction

Layered double hydroxides (LDHs), Two-dimensional (2D) nanomaterials with sheet-like structures, are a class of ionic solids characterized by their layered structure, which adheres to the general sequence [AcB Z AcB]_n. In this structure, c represents layers of metal cations, while A and B denote layers of hydroxide (OH-) anions, and Z includes layers of other anions and neutral molecules (such as water). Lateral offsets between the layers can result in longer repeating periods [1]. They stand out as an emerging and versatile class of inorganic layered nanomaterials, as well as natural or synthetic anionic clay minerals, characterized by the general formula [M_{1-x}²⁺ M_x³⁺ (OH)₂] ^{x+} (Anⁿ⁻)_{x/n} • mH₂O₁ where M2+ represents a divalent metal ion (e.g., Mg2+, Ni2+, etc.), M3+ denotes a trivalent metal ion (e.g., Al³⁺, Cr³⁺, etc.), Anⁿ⁻ is an anion (e.g., CO₃²⁻, Cl⁻, etc.), and the charge density of the LDH layers is determined by $x = M^{3+}/(M^{2+} + M^{3+})$, with values typically ranging from 0.2 to 0.33 for pure LDH phases [2]. LDHs are potential candidate nanomaterials for several applications as environmental applications (adsorbents and sensors), catalysis, magnetization, biomedical science (drug delivery), electrochemistry, polymerization, controlled release formulation and photochemistry [3] due to their outstanding structural and physicochemical properties. The activity and broader applications of LDHs are constrained by the absence of functional groups and structural components in pure LDHs. To address these limitations, modified LDHs have been developed by incorporating functional groups or structural elements. These modifications aim to create novel functional LDH-based catalysts. In this context, the presence of hydroxyl groups on the surface and the positively charged [Mg(OH)6] octahedra allows LDHs to interact both electrostatically and chemically with various functional groups or structural components [4, 5]. Additionally, several modification strategies for LDHs have been proposed, including the incorporation of metal nanoparticles, metal oxides, polyoxometalates (POMs), carbon-based nanomaterials, and intercalation techniques [6-8].

The immobilization of metallic nanoparticles (e.g., Au, Pt, Pd, etc.) onto LDHs results in the formation of nanocomposites (NCs) with enhanced characteristics and reactivity. The interaction between metal NPs and LDHs, along with the synergy between the metal and LDHs, imparts significant advantages to the resulting NCs [9]. Metal nanoparticle-LDH nanocomposites are commonly employed as catalysts in various chemical industrial reactions, such as catalytic oxidation and hydrogenation, electrocatalysis, and photocatalysis [10]. Gevers et al. made a comparison nano-structured transition metal modified tri-metal MgMAl-LDHs (M = Fe, Zn, Cu, Ni, Co) on the influence of the quantity and type of transition metals (TMs) incorporated into the LDH layers, with an emphasis on purity, structural differences, morphological variations, and differences in thermal stability, all while synthesizing the LDHs under identical conditions [11]. Mostly, modifying LDHs by transition metal effects their textural properties and therefore changes their performance in different applications. LDHs are most commonly synthesized through co-precipitation, which is favored for its simplicity and the high purity of the resulting LDHs [11]. Alternative methods include urea hydrolysis, sol-gel synthesis, and hydrothermal synthesis [12].

El-Naggar et al 3 of 13

2. Materials and Methods

2.1. Materials and chemicals

All reagents used in this study were of analytical grade quality. Magnesium chloride hexahydrate (MgCl₂·6H₂O) (98.0% pure), cupric chloride (CuCl₂) (97.0% pure), and sodium tungstate (H₄Na₂O₆W) were obtained from El Nasr Pharmaceutical Chemicals Co. Ferric chloride hexahydrate (FeCl₃·6H₂O) (99.0% pure) was sourced from Egypt Chemicals. Sodium hydroxide (NaOH) (97.0% pure) and hydrochloric acid (HCl) were purchased from NATCO Laboratory Chemicals Reagent. Sodium carbonate (Na₂CO₃) (99.8% pure) was acquired by Alfa Chemical Group. All solutions were prepared using deionized (DI) water with a resistivity of 18 M Ω /cm³, which was also used for rinsing and cleaning. All chemicals were used directly in this study without further purification.

2.2. Synthesis Methods

2.2.1. Preparation of Mg/Fe LDH

Mg/Fe-LDH was synthesized using a co-precipitation method. In accordance with standard procedures outlined in the literature [13, 14], (FeCl₃·6H₂O) and (MgCl₂·6H₂O) solutions was mixed together in molar ratio of Mg²⁺ to Fe³⁺ ions of 2:1. A mixture of 1 M NaOH and 1 M Na₂CO₃ in a volume ratio of 3:1 was added dropwise to the solution until the pH reached approximately 10, while continuously stirring for one hour. The resulting mixture was aged 24 hours at 70 °C. The precipitate was then filtered and thoroughly rinsed with deionized water multiple times to remove chloride content, dried at 60 °C overnight, and finely ground.

2.2.2. Preparation of Cu and W Modified Mg/Fe-LDH

Cu/Mg/Fe (1:1:1) and W/Mg/Fe (1:1:1) LDH solutions were prepared. The pH of both solutions was adjusted to approximately 10 by gradually adding a mixture of 1 M NaOH and 1 M Na₂CO₃ in a volume ratio of 3:1 while stirring continuously for one hour. The resulting mixtures were allowed to age for 24 hours at 70 °C. The precipitates were then filtered, rinsed with ultrapure water, and dried overnight at 70 °C. Following this, the prepared LDH samples were symbolized as MgFe, CuMgFe, and WMgFe LDHs.

2.3. LDH characterization

Thermogravimetric analysis (TGA) was conducted using a V2-2A DUPONT 9900 thermal analyzer, with α -Al₂O₃ serving as a reference material, to examine the thermal behavior of the prepared samples across a temperature range from room temperature to 1000 °C in a static air environment. TG measurements were performed on samples weighing between 5 and 15 mg at a heating rate of 10 °C/min. The crystal phases of the synthesized LDH were characterized using an X-ray diffractometer (XRD; JSX-60PA/Jeol, Japan). Morphological features were analyzed using a scanning electron microscope (SEM, FEGSEM, THERMOSCIENTIFIC QUATTRO S.). Textural properties, including Brunauer-Emmett-Teller surface area (SBET) and total pore volume (VTotal), were determined from N₂ adsorption/desorption isotherms at -196 °C using a NOVA 3000 high-speed gas sorption analyzer (version 6.10, Quantachrome Corporation, USA).

El-Naggar et al 4 of 13

3. Results and Discussion

3.1 Characterization

3.1.1 Thermogravimetric Analysis

Thermogravimetric analysis for all three LDH samples is presented in Figure 1. All samples exhibit multistep weight lose mass (typical for LDHs): an initial weight loss at low temperature (physiosorbed water), one or more mid-temperature losses (interlayer water + dehydroxylation), and a higher-temperature loss associated with LDH decomposition / collapse to mixed oxides. W/Mg/Fe shows the smallest total mass loss and a clear plateau at high temperature which exposes highest thermal stability and highest final residue (heavy W-oxide contribution). Cu/Mg/Fe shows the largest mass loss (especially through the mid to high temperature region) and additional structure in the curve lowest thermal stability; Cu appears to accelerate decomposition (catalytic effect) or increase labile chloride/hydroxyl removal. Mg/Fe LDH sits between them (overlaps early with others) baseline LDH behavior. At Room to ~150 °C (first small drop); assigned to loss of adsorbed and surface water and loosely bound interlayer water. All samples show this; magnitude slightly higher for Cu and W samples if they retain more physiosorbed water after synthesis. At $\sim 150 \rightarrow 300$ °C (first major loss); removal of interlayer water + beginning of partial dehydroxylation of brucite-like layers. Here, a significant mass drop in all curves was shown; Cu sample often shows a sharper step (more labile interlayer species). the second stage of weight loss at ~300 \rightarrow 500(-600) °C; dehydroxylation of layers and decomposition of interlayer carbonate; collapse of layered structure to mixed oxides. This is where the Cu/Mg/Fe loses the most mass — large and continuous loss — indicating either more carbonate content or that Cu catalyzes the dehydroxylation/carbonate decomposition. The W/Mg/Fe shows a smoother, smaller loss here and then levels off indicates greater structural stability and heavier oxide residue (WO3) remains. The last mass loss at > ~600 °C; plateau corresponds to final oxide residue. WMgFe LDH sample retains the highest % residue (W oxide heavy), CuMgFe sample retains the least (more volatile mass lost earlier or lower metal oxide fraction). The final residue composition likely: MgO + $Fe_2O_3 + (WO_3 \text{ or } CuO/Cu_2O)$ depending on dopant and redox changes [15, 16].

El-Naggar et al 5 of 13

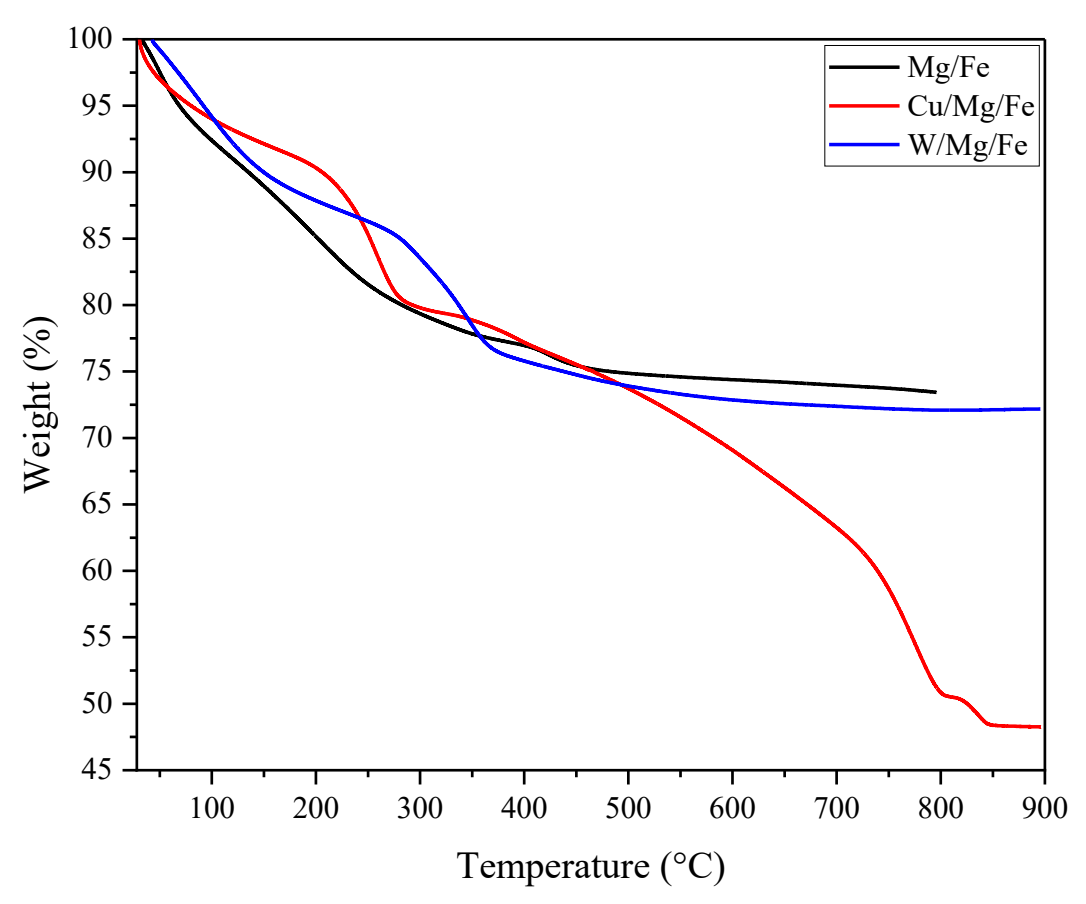


Fig. 1. TGA for Mg/Fe, Cu/Mg/Fe and W/Mg/Fe LDHs.

3.1.2 X-Ray Diffraction

The crystal structure of the prepared samples was examined using XRD (Fig. 2). In Figure. 2, all XRD patterns samples of the three samples confirm the formation of well-crystallized with sharp and symmetric reflections at low angles corresponding to the basal spacing of (003), (006) and (012) which characteristic of the hydrotalcite (Rhombohedral phase and its symmetry is R-3m), confirmed the development of a well-crystallized layered structure [17] as shown in table 1. In addition to these peaks, there are other peaks like: for Mg/Fe-LDH: at $2\theta = 61^{\circ}$ Corresponding to (440) with d-spacing 1.55 Å, which is distinguishing MgFe₂O₄ (PDF#01-085-9166, cubic spinel phase and its space group Fd-3m). And also, for Cu/Mg/Fe- LDH: ferric oxide (Fe₂O₃) at 2θ = 27.61° corresponding to (112) with d-spacing 3.23 (PDF# 00-058-0266, Orthorhombic phase, and its space group Pna21). The XRD results indicate that the Cu/Mg/Fe LDH exhibits superior crystallinity compared to other samples. The average crystallite size according to Sherrer equation (Eq. 1) was calculated and cited in Table 1. Substitution with transition metals (Cu and W) significantly affects the crystallinity and peak sharpness, increase in average crystallite size is observed upon metal substitution: from 9.9 nm (Mg/Fe-LDH) to 62.7 nm (Cu/Mg/Fe-LDH) and 70.6 nm (W/Mg/Fe-LDH). This implies that the addition of Cu²⁺ and W⁶⁺ ions promote crystal growth and improves structural ordering, likely due to changes in nucleation and growth kinetics during synthesis.

El-Naggar et al 6 of 13

$$D_{hkl} = \frac{\kappa \lambda}{\beta_{hkl} \cos \theta} \tag{1}$$

where:

- D_{hkl} = crystallite size corresponding to the diffraction plane (hkl),
- $K = \text{shape factor (usually } \approx 0.9),$
- λ = X-ray wavelength (for Cu K α radiation, λ = 1.5406 Å),
- β_{hkl} = full width at half maximum (FWHM) of the diffraction peak (in radians),
- θ = Bragg angle (in degrees or radians).

Table 1. XRD parameters; Miller indices for LDH samples, 2θ, d-spacing and average crystallite size.

| LDH sample | Miller indices characteristic for LDH | d-spacing [Å] | | Average crystallite | |
|--------------|---------------------------------------|---------------|------|---------------------|--|
| LDH Sample | (hkl) | 20() | | size (nm) | |
| Mg/Fe-LDH | (003) | 11.58 | 7.63 | | |
| | (006) | 23.2 | 3.83 | 9.9 | |
| | (012) | 34.52 | 2.6 | | |
| Cu/Mg/Fe-LDH | (003) | 11.62 | 7.61 | | |
| | (006) | 24.48 | 3.63 | 62.7 | |
| | (012) | 35.78 | 2.51 | | |
| W/Mg/Fe-LDH | (003) | 11.73 | 7.54 | | |
| | (006) | 23.4 | 3.8 | 70.6 | |
| | (012) | 34.4 | 2.61 | | |

El-Naggar et al 7 of 13

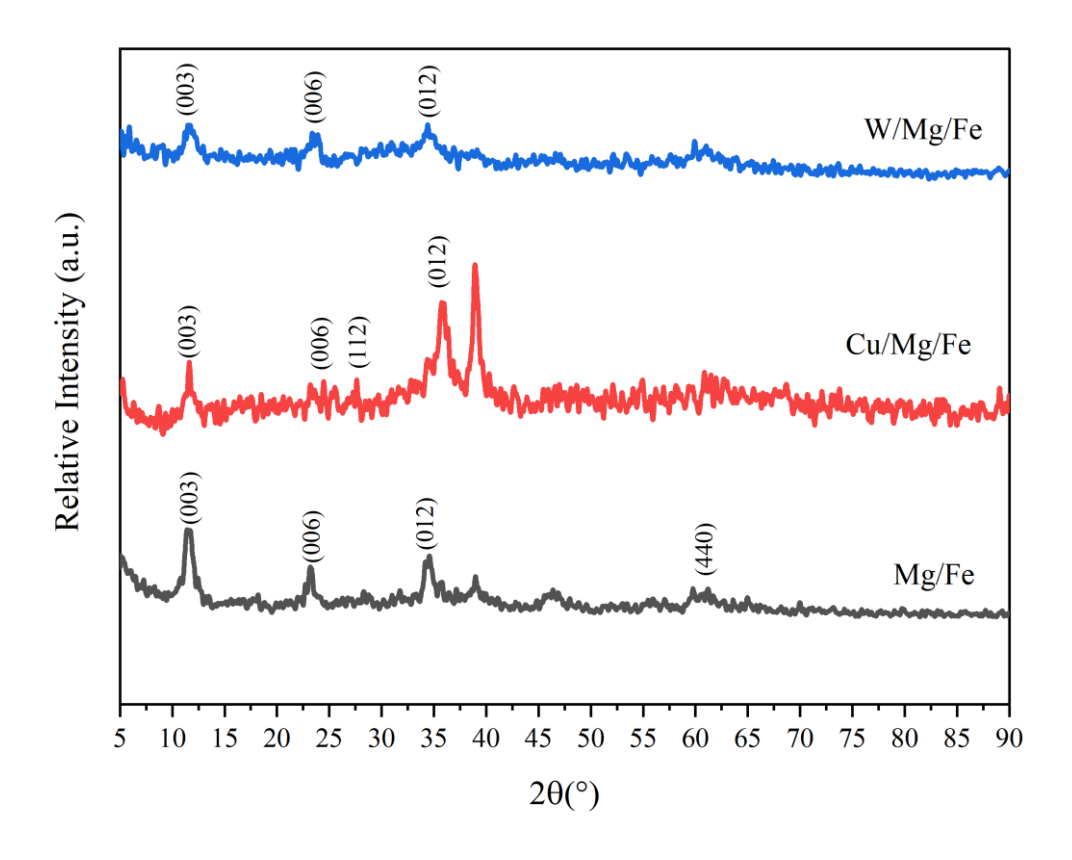


Fig. 2. XRD patterns of the LDH samples.

3.1.3 Scan Electron Microscope images

SEM technique was employed to examine the morphological properties of the synthesized materials. The SEM images of the LDH samples are presented in Figure 3. The SEM micrograph of MgFe LDH (Fig. 3a) shows irregularly shaped, aggregated plate-like structures typical of layered double hydroxides. The particles are loosely packed with noticeable voids and rough surfaces, indicating a less crystalline and less compact morphology. This suggests that the pristine Mg/Fe-LDH has a heterogeneous particle distribution and possibly smaller crystallite size, consistent with the XRD result (≈9.9 nm).

The Cu-modified LDH (Fig. 3b) exhibits a denser and more uniform morphology, with flower-like or flake-assembled structures formed by agglomerated nanosheets. The surface appears smoother and more compact than that of Mg/Fe-LDH, suggesting enhanced crystallinity and better particle intergrowth. The presence of Cu²+ likely promotes nucleation and structural ordering, resulting in larger crystallites (≈62.7 nm, as confirmed by XRD).

The W-containing LDH (Fig. 3c) displays well-defined, spherical-like or clustered nanostructures with smaller, densely packed grains, forming a highly uniform and compact morphology. This indicates a significant improvement in particle interconnection and crystallite growth, consistent with the largest crystallite size (≈70.6 nm). The incor-

El-Naggar et al 8 of 13

poration of W⁶⁺ ions may enhance electrostatic interactions and layer stacking, promoting crystal growth and surface uniformity.

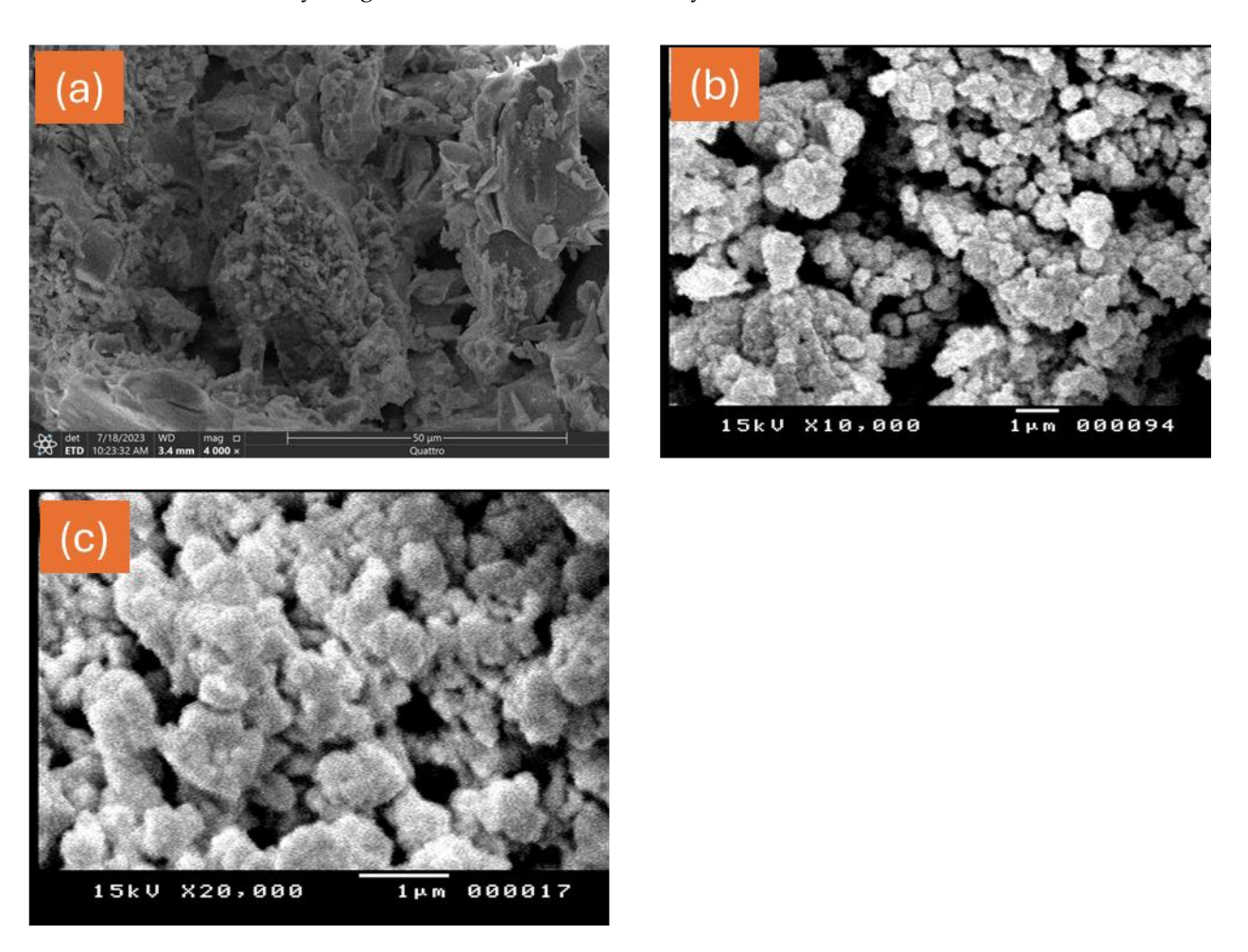


Fig. 3. SEM for (a) MgFe, (b) CuMgFe and (c) WMgFe LDH samples

3.1.4 N₂-Adsorption-Desorption

BET Isotherms

The textural features of the LDH samples, including surface area, pore volume, pore radius, and BJH pore size distribution, were investigated through N_2 adsorption–desorption measurements at -196 °C. All samples exhibited type IV isotherms in accordance with the IUPAC classification [18], characteristic of materials containing micro- and mesopores. The Mg/Fe-LDH displayed an H3-type loop, typically associated with slit- or wedge-shaped pores resulting from stacked plate-like particles and capillary condensation within mesopores [19]. In contrast, the Cu/Mg/Fe and W/Mg/Fe samples exhibited H4-type hysteresis loops, indicating the development of narrow slit-like mesopores derived from the aggregation of lamellar sheets [20].

As shown in the adsorption isotherms (Fig. 4a), a clear difference in N_2 uptake is observed among the samples. The W/Mg/Fe material records the highest adsorption over the entire relative-pressure range, while Cu/Mg/Fe and Mg/Fe show progressively lower

El-Naggar et al 9 of 13

uptakes. The gradual rise in adsorbed volume with increasing P/P° reflects the dominance of mesoporosity [21], characterized by multilayer adsorption and capillary condensation. The pronounced slope of the WMgFe sample suggests enhanced pore accessibility and larger pore volume, whereas the passive uptake of the CuMgFe LDH indicates partial pore blocking and denser particle packing, which limit nitrogen diffusion through the pore structure.

Pore size distribution

The pore-size distribution (Fig. 4b) confirms that all samples show main contributions in the mesopore range (~20–40 Å), but the W/Mg/Fe sample displays a stronger, sharper peak (especially near ~30 Å), indicating a larger population of fairly uniform mesopores. The Cu/Mg/Fe sample has a broader, lower intensity distribution consistent with fewer and more variable mesopores, while the Mg/Fe sample shows the smallest $\Delta V/\Delta r$ signals across radii, supporting its low pore volume and limited mesoporosity.

t-Plots

The t-plot (Fig. 4c) shows the relationship between the adsorbed N_2 volume and statistical film thickness, providing insight into the microporous and external surface area of the samples. The W/Mg/Fe-LDH exhibits the steepest slope and highest intercept, indicating the largest total pore volume and external surface area, while Mg/Fe-LDH shows moderate adsorption and Cu/Mg/Fe-LDH the lowest. The nearly linear trends at higher thickness values suggest a predominance of mesoporous structures, with limited micropore contribution [22]. The significantly higher adsorption of W/Mg/Fe-LDH confirms that tungsten incorporation enhances the formation of textural porosity, possibly through distortion of LDH layers and generation of interparticle voids.

as-Plots

Similarly, the α_s -plot (Fig. 4d)—which relates the adsorbed volume to the relative surface area—supports these observations. The W/Mg/Fe-LDH again demonstrates the highest adsorbed volume across the α_s range, confirming a well-developed porous network and enhanced surface accessibility. In contrast, Cu/Mg/Fe-LDH exhibits the lowest adsorption, implying reduced surface area and denser particle aggregation, consistent with its compact morphology observed by SEM. These results collectively indicate that metal substitution notably alters the LDH textural properties: W incorporation increases surface area and pore volume, while Cu incorporation decreases them, correlating with the observed variations in crystallite size and microstructure.

Textural data

Correlating isotherms (Fig. 4a) and PSD (Fig. 4b) with the t-plot (Fig. 4c) and α_s -plot (Fig. 4d) produces a consistent picture: the W-doped material shows the highest adsorbed volumes, the largest external/total pore contribution in the t-plot and the greatest relative surface accessibility in the α_s -plot, all pointing to a well-developed mesopore network and high accessible surface area. Mg/Fe sits between the extremes (moderate uptake and broader pore sizes), while Cu/Mg/Fe consistently shows the poorest textural development (lowest uptake, lowest pore volume, and smallest α_s response), which explains its

El-Naggar et al

low BET surface area and suggests densification or interparticle sintering/aggregation that blocks pores. Together these four plots demonstrate that metal substitution modifies LDH textural properties: W promotes formation of uniform mesopores and high accessibility, whereas Cu promotes densification and reduced accessible porosity.

The BET analysis results (Table 2) reveal that the specific surface area (S_{BET}), total pore volume (V_P), and average pore radius (r_P) vary notably with metal substitution in Mg/Fe-LDH. The pristine Mg/Fe-LDH shows the highest surface area (87 m²/g) and largest pore volume (0.086 cm³/g), indicating a well-developed mesoporous structure that facilitates gas adsorption. Its relatively large pore radius (22.3 Å) suggests a predominance of mesopores, consistent with the gradual slope observed in the t- and α s-plots. In contrast, the Cu/Mg/Fe-LDH exhibits a dramatic decrease in both surface area (14 m²/g) and pore volume (0.015 cm³/g), implying that Cu incorporation leads to denser aggregation and pore blocking within the LDH framework. The slightly smaller pore size (20 Å) supports the formation of more compact structures, as observed in the SEM images. Conversely, the W/Mg/Fe-LDH sample displays an intermediate surface area (38 m²/g) and pore volume (0.050 cm³/g), suggesting that tungsten enhances structural compactness while still maintaining accessible porosity. The smaller pore radius (17.4 Å) indicates a shift toward narrower mesopores, consistent with its highly crystalline and uniform morphology.

Table 2. Textural data for the LDHs.

| Sample | Свет | SBET (m ² /g) | St (m ² /g) | V _P (cc/g) | rp (Å) |
|----------|------|--------------------------|------------------------|-----------------------|--------|
| Mg/Fe | 15.4 | 87 | 81 | 0.086 | 22.3 |
| Cu/Mg/Fe | 30.6 | 14 | 13.6 | 0.015 | 20 |
| W/Mg/Fe | 12 | 38 | 36.2 | 0.050 | 17.4 |

El-Naggar et al

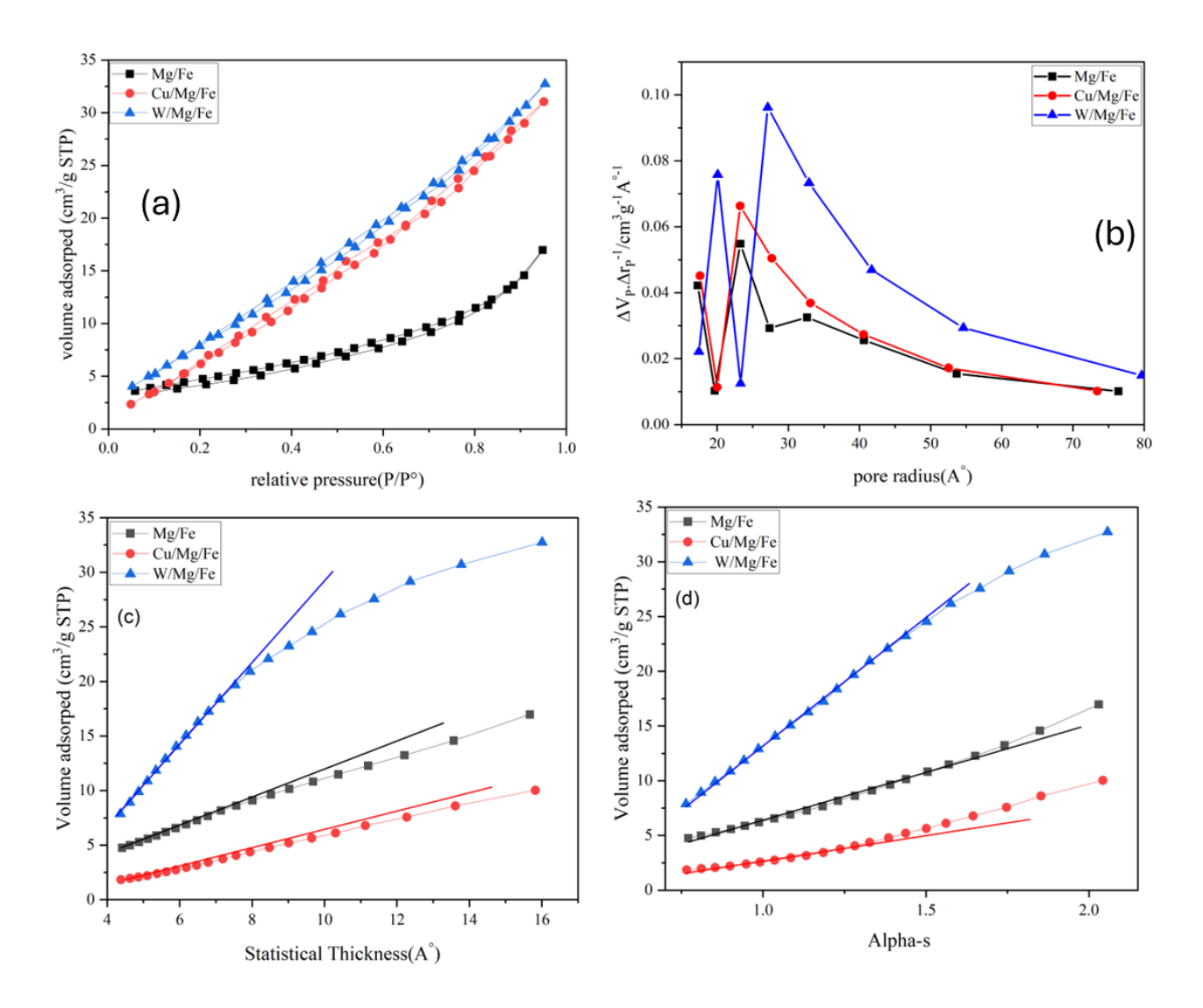


Fig. 4: (a) N₂ adsorption/desorption/desorption isotherm, (b) pore size distribution curves, (c) t-plots and (d) αs-plots for Mg/Fe, Cu/Mg/Fe and W/Mg/Fe LDHs respectively.

4. Conclusions

Mg/Fe-LDH and its Cu- and W-modified derivatives were successfully synthesized via the co-precipitation method, yielding well-crystallized hydrotalcite-like structures. Structural characterization results confirmed that metal substitution significantly influenced the structural, morphological, and textural properties of the LDHs. XRD confirmed the preservation of the layered double hydroxide phase, while Cu²⁺ and W⁶⁺ incorporation promoted crystal growth and increased crystallite size. SEM observations showed that Cu addition led to compact, flake-like aggregates, whereas W incorporation produced highly uniform, densely packed nanostructures. Thermal analysis demonstrated that W/Mg/Fe-LDH exhibited the greatest thermal stability, attributed to the formation of thermally robust tungsten oxides, while Cu/Mg/Fe-LDH showed accelerated decomposition due to the catalytic role of copper. BET and pore analyses indicated that W doping enhanced mesoporosity and accessible surface area, leading to improved pore connectivity, while Cu doping caused pore blockage and reduced surface accessibility. Overall,

El-Naggar et al 12 of 13

metal substitution effectively tuned the crystallinity, morphology, and textural characteristics of Mg/Fe-LDH, with W incorporation enhancing structural order and porosity, and Cu incorporation promoting densification and decreased surface area.

References

- 1. Evans, D.G. and R.C. Slade, Structural aspects of layered double hydroxides. Layered double hydroxides, 2006: p. 1-87.
- 2. Taviot Guého, C., V. Prévot, C. Forano, G. Renaudin, C. Mousty, and F. Leroux, *Tailoring hybrid layered double hydroxides* for the development of innovative applications. Advanced Functional Materials, 2018. **28**(27): p. 1703868.
- 3. dos Santos Lins, P.V., D.C. Henrique, A.H. Ide, C.L. de Paiva e Silva Zanta, and L. Meili, *Evaluation of caffeine adsorption by MgAl-LDH/biochar composite*. Environmental Science and Pollution Research, 2019. **26**(31): p. 31804-31811.
- 4. Laipan, M., R. Zhu, J. Zhu, and H. He, Visible light assisted Fenton-like degradation of Orange II on Ni3Fe/Fe3O4 magnetic catalyst prepared from spent FeNi layered double hydroxide. Journal of Molecular Catalysis A: Chemical, 2016. 415: p. 9-16.
- 5. Tang, Z., Z. Qiu, S. Lu, and X. Shi, Functionalized layered double hydroxide applied to heavy metal ions absorption: A review. Nanotechnology Reviews, 2020. **9**(1): p. 800-819.
- 6. Lu, H., Z. Zhu, H. Zhang, J. Zhu, Y. Qiu, L. Zhu, and S. Küppers, Fenton-like catalysis and oxidation/adsorption performances of acetaminophen and arsenic pollutants in water on a multimetal Cu–Zn–Fe-LDH. ACS applied materials & interfaces, 2016. 8(38): p. 25343-25352.
- 7. Nayak, S., G. Swain, and K. Parida, Enhanced photocatalytic activities of RhB degradation and H2 evolution from in situ formation of the electrostatic heterostructure MoS2/NiFe LDH nanocomposite through the Z-Scheme mechanism via p–n heterojunctions. ACS applied materials & interfaces, 2019. 11(23): p. 20923-20942.
- 8. Cai, T., P. Zhang, X. Shen, E. Huang, X. Shen, J. Shi, Z. Wang, and Q. Sun, *Synthesis of Pt-loaded NiFe-LDH nanosheets on wood veneer for efficient gaseous formaldehyde degradation*. ACS applied materials & interfaces, 2020. **12**(33): p. 37147-37154.
- 9. Fan, G., F. Li, D.G. Evans, and X. Duan, Catalytic applications of layered double hydroxides: recent advances and perspectives. Chemical Society Reviews, 2014. **43**(20): p. 7040-7066.
- 10. Li, Z., M. Chen, H. Hu, Q. Zhang, and D. Tao, Mechanochemical synthesis of novel Pt modified ZnAl-LDH for effective ciprofloxacin photodegradation. Journal of Solid State Chemistry, 2020. 290: p. 121594.
- 11. Gevers, B.R., S. Naseem, A. Leuteritz, and F.J. Labuschagné, *Comparison of nano-structured transition metal modified tri-metal MgMAl–LDHs* (M= Fe, Zn, Cu, Ni, Co) prepared using co-precipitation. RSC advances, 2019. **9**(48): p. 28262-28275.
- 12. Duan, X. and D.G. Evans, Layered double hydroxides. Vol. 119. 2006: Springer Science & Business Media.
- 13. Nuryadin, A. and T. Imai, Application of amorphous zirconium (hydr) oxide/MgFe layered double hydroxides composite in fixed-bed column for phosphate removal from water. Global Journal of Environmental Science and Management, 2021. 7(4): p. 485-502.
- 14. Chen, Q., Z. Cheng, X. Li, C. Wang, L. Yan, G. Shen, and Z. Shen, *Degradation mechanism and QSAR models of antibiotic contaminants in soil by MgFe-LDH engineered biochar activating urea-hydrogen peroxide*. Applied Catalysis B: Environmental, 2022. 302: p. 120866.
- 15. Cardinale, A.M., M. Fortunato, F. Locardi, and N. Parodi, *Thermal analysis of MgFe-Cl Layered doubled hydroxide (LDH) directly synthetized and produced "via memory effect"*. Journal of Thermal Analysis and Calorimetry, 2022. **147**(9): p. 5297-5302.
- 16. Manzar, M.S., P. Palaniandy, J. Georgin, D.S.P. Franco, M. Zubair, N.D. Muazu, W. Faisal, and N. El Messaoudi, *Synthesis of LDH-MgAl and LDH-MgFe composites for the efficient removal of the antibiotic from water*. Environmental Science and Pollution Research, 2024. **31**(43): p. 55577-55596.

El-Naggar et al 13 of 13

17. Harizi, I., D. Chebli, A. Bouguettoucha, S. Rohani, and A. Amrane, *A new Mg–Al–Cu–Fe-LDH composite to enhance the adsorption of acid red 66 dye: Characterization, kinetics and isotherm analysis*. Arabian Journal for Science and Engineering, 2019. 44: p. 5245-5261.

- 18. Zheng, C., X. Yang, M. Li, and S. Bai, Bridging the adsorption data and adsorption process by introducing a polynomial structure to accurately describe IUPAC isotherms, stepwise isotherms, and stepwise breakthrough curves. Langmuir, 2024. 40(8): p. 4132-4141.
- 19. Mel'gunov, M.S., Application of the simple Bayesian classifier for the N2 (77 K) adsorption/desorption hysteresis loop recognition. Adsorption, 2023. **29**(5): p. 199-208.
- 20. Chandrabose, V., J.W. Park, S.Y. Jung, K.K. Wang, and J.-M. Oh, *Highly porous layered double hydroxide and mixed metal oxide by sacrificial bio-template, egg white foam.* Crystals, 2023. **13**(11): p. 1603.
- 21. Buttersack, C., Modeling of type IV and V sigmoidal adsorption isotherms. Physical Chemistry Chemical Physics, 2019. **21**(10): p. 5614-5626.
- 22. Bhambhani, M., P. Cutting, K. Sing, and D. Turk, *Analysis of nitrogen adsorption isotherms on porous and nonporous silicas by the BET and αs methods*. Journal of Colloid and Interface Science, 1972. **38**(1): p. 109-117.